Letter

Relaxation in dipolar spin ladders: From pair production to false-vacuum decay

Gustavo A. Domínguez-Castro,[1] Thomas Bilitewski,[2] David Wellnitz,[3,4] Ana Maria Rey,[3,4] and Luis Santos[1]

[1]*Institut für Theoretische Physik, Leibniz Universität Hannover, Appelstrasse 2, D-30167 Hannover, Germany*
[2]*Department of Physics, Oklahoma State University, Stillwater, Oklahoma 74078, USA*
[3]*JILA, National Institute of Standards and Technology and Department of Physics, University of Colorado, Boulder, Colorado 80309, USA*
[4]*Center for Theory of Quantum Matter, University of Colorado, Boulder, Colorado 80309, USA*

(Received 18 January 2024; accepted 31 July 2024; published 15 August 2024)

Ultracold dipolar particles pinned in optical lattices or tweezers provide an excellent platform for the study of the intriguing equilibration dynamics of spin models with dipolar exchange. Starting with an initial state in which spins of opposite orientation are prepared in each of the legs of a ladder lattice, we show that spin relaxation displays an unexpected dependence on interleg distance and dipole orientation. This dependence, stemming from the interplay between intra- and interleg interactions, results in three distinct relaxation regimes: (i) ergodic, characterized by the fast relaxation towards equilibrium of correlated pairs of excitations generated at exponentially fast rates from the initial state; (ii) metastable, in which the state is quasilocalized in the initial state and only decays in exceedingly long timescales, resembling false-vacuum decay; and, surprisingly, (iii) partially relaxed, with coexisting fast partial relaxation and partial quasilocalization. The realization of this intriguing dynamics is at hand in current state-of-the-art experiments in dipolar gases.

DOI: 10.1103/PhysRevA.110.L021302

Introduction. Quantum simulators using ultracold gases in optical potentials have dramatically improved our understanding of many-body quantum dynamics, as highlighted by recent experiments on many-body localization [1–3], quantum scars [4], or Hilbert-space fragmentation [5,6]. Up to recently, nearest-neighbor spin interactions only resulted from relatively weak superexchange processes [7–17]. This is changing due to rapid progress in the realization of dipole-mediated spin interactions in various physical systems, including magnetic atoms [18–24], Rydberg atoms [25–28], and polar molecules [29–31]. In parallel, the development of optical tweezers [32–35] and quantum gas microscopes for polar molecules [36] opens fascinating perspectives for unveiling the intriguing dynamics of dipolar spin models resulting from the long-range anisotropic dipole-dipole interactions.

Exploring nonequilibrium dynamics in dipolar spin models is further facilitated by the capability to controllably prepare layered arrays with nontrivial initial spin distributions [17,37–40]. For polar molecules this was demonstrated in recent experiments where each layer was initialized in opposite spin states (encoded in rotational levels) [41]. This case is particularly interesting since dipolar exchange results in the correlated creation of spin excitations in each layer [42,43], resembling pair creation from vacuum fluctuations, or parametric amplification and two-mode squeezing in quantum optics [44,45].

Although in contrast to integrable [46] and many-body localized systems [47] nonintegrable ones are expected to eventually thermalize [48], they may do so after a possibly long transient prethermalization stage, which has been the focus of major attention [48–50]. Long-lived metastable states also appear in so-called false-vacuum decay, a phenomena first investigated in the context of quantum field theories with applications in cosmology and theory of fundamental interactions [51], which has been predicted in quantum spin chains [52,53] and has been recently observed in ferromagnetic superfluids [54]. Ladder lattices provide a convenient system to study relaxation dynamics [37,38,40,55,56], as they are theoretically tractable, while still displaying interesting physics.

In this Letter, we show that experimentally feasible ladders of spin-$1/2$ pinned dipoles [Fig. 1(a)] present a highly nontrivial relaxation dynamics, characterized by an anomalously long-lived prethermal stage. We illustrate this for the particular experimentally relevant case in which the spins in each leg are initialized in opposite orientations, which may be subsequently admixed by interchain dipolar exchanges. We focus on whether and how the initial pattern relaxes towards an equilibrium state characterized by an average zero magnetization in both legs. It might be expected that relaxation is fastest when the interleg dipolar exchange is maximal, i.e., for dipoles oriented perpendicular to the ladder axis [$\theta = 0$ in Fig. 1(a)], and that increasing the interchain separation Δ only trivially enlarges the timescale of relaxation, without modifying its qualitative nature.

Interestingly, none of these *a priori* reasonable expectations are correct, illustrating the highly nontrivial nature of the dynamics of dipolar spins. We show that spin relaxation is maximally favored at the dipole orientation for which there is no spin exchange along the legs. Moreover, increasing Δ does not only enlarge the relaxation timescale, but changes qualitatively the long-time evolution, leading to three distinct relaxation regimes. The ergodic regime, at low Δ, is characterized by an exponential creation of correlated pairs of spin excitations at short times, followed by a fast relaxation towards equilibrium. At large Δ, the system is in a highly metastable, quasilocalized regime, remaining in the initial state and only relaxing in an exceedingly long timescale

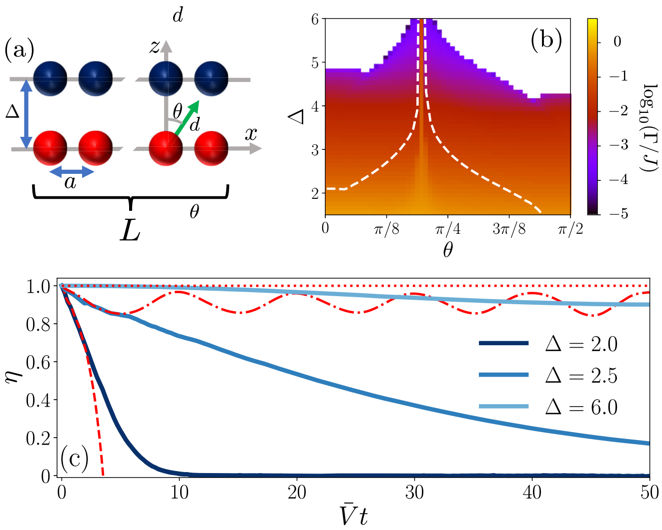

FIG. 1. (a) Sketch of the ladder model. Spins in each leg are initially prepared with opposite orientations (red and blue balls). (b) Instability rate Γ for a ladder of $L = 1001$ rungs, as a function of the orientation θ and the separation Δ. The colored region indicates where at least one momentum mode is unstable. The dashed curve is the effective instability threshold for $L = 11$. (c) Imbalance evolution for $\theta = 0$ and $\Delta = 2$, 2.5, and 6 ($a = 1$); dashed, dash-dotted, and dotted red curves depict the Bogoliubov predictions for each case, respectively.

resembling false-vacuum decay [51–54]. Remarkably, at intermediate Δ, the system is in a partially relaxed regime, with coexisting partial equilibration and very long-lived partial quasilocalization. Moreover, the three relaxation regimes present as well a markedly different evolution of the entanglement entropy [57]. The observation of these dynamics is well within reach of present experiments.

Model. We consider two parallel spin-1/2 chains of L sites, denoted as A and B. The chains are characterized by a lattice spacing a, set to $a = 1$ below, and are separated by a distance Δ [Fig. 1(a)]. We assume $\Delta > a$. Due to resonant electric dipole-dipole interactions, at zero electric field the spins undergo both intraleg and interleg exchange interactions. The system is then described by the following Hamiltonian:

$$\hat{H} = \sum_{\alpha=A,B} \sum_{i>j} V_{ij}^{\alpha\alpha}(\hat{s}_{i\alpha}^{+}\hat{s}_{j\alpha}^{-} + \hat{s}_{i\alpha}^{-}\hat{s}_{j\alpha}^{+}) + \sum_{i,j} V_{ij}^{AB}(\hat{s}_{iA}^{+}\hat{s}_{jB}^{-} + \hat{s}_{iA}^{-}\hat{s}_{jB}^{+}), \quad (1)$$

with $\hat{s}_i^{\alpha} = \hat{\sigma}_i^{\alpha}/2$ being the spin operators in terms of the Pauli matrices $\hat{\sigma}_i^{x,y,z}$ that act on the spin at site i. We focus our attention below on exchange couplings of the form

$$V_{ij}^{\alpha\alpha'} = \frac{J}{\left|\mathbf{r}_i^{\alpha} - \mathbf{r}_j^{\alpha'}\right|^3}\left(1 - \frac{3\left[\hat{e}_d \cdot (\mathbf{r}_i^{\alpha} - \mathbf{r}_j^{\alpha'})\right]^2}{\left|\mathbf{r}_i^{\alpha} - \mathbf{r}_j^{\alpha'}\right|^2}\right), \quad (2)$$

where J is the spin-exchange rate (proportional to the dipole moment squared); $\hat{e}_d = \hat{e}_z \cos\theta + \hat{e}_x \sin\theta$ characterizes the dipole orientation, fixed by an external magnetic field; and $\mathbf{r}_i^{\alpha}$ is the position of site i of chain α. Motivated by recent works on polar molecules in bilayers [41], we consider all spins in A (B) initially in spin $\uparrow$ ($\downarrow$). Below, we study the stability of elementary spin excitations on top of the initial pattern, which characterizes short timescales, and then address whether and how the system reaches equilibrium in longer times.

Stability analysis. At short times, deviations from the initial condition are best analyzed using the Holstein-Primakoff transformation $\hat{s}_{A,i}^{z} = 1/2 - \hat{a}_i^{\dagger}\hat{a}_i$, $\hat{s}_{A,i}^{+} = \hat{a}_i$, $\hat{s}_{B,i}^{z} = -1/2 + \hat{b}_i^{\dagger}\hat{b}_i$, and $\hat{s}_{B,i}^{-} = \hat{b}_i$, which maps the initial spin pattern to a vacuum of spin excitations [58]. The hard-core boson operator $\hat{a}_i^{\dagger}$ ($\hat{b}_i^{\dagger}$) creates a spin excitation at site i in leg A (B). For low density of spin excitations, the hard-core nature can be neglected, and the Hamiltonian may be re-expressed in quasimomentum space as

$$\hat{H} = \sum_k [\varepsilon_k(\hat{a}_k^{\dagger}\hat{a}_k + \hat{b}_k^{\dagger}\hat{b}_k) + \Omega_k\hat{a}_k^{\dagger}\hat{b}_{-k}^{\dagger} + \Omega_k^{*}\hat{b}_{-k}\hat{a}_k], \quad (3)$$

where $\hat{a}_k = \frac{1}{\sqrt{L}}\sum_j e^{-ikj}\hat{a}_j$ and $\hat{b}_k = \frac{1}{\sqrt{L}}\sum_j e^{-ikj}\hat{b}_j$. Neglecting the hard-core constraint fails at longer times. Nevertheless, Eq. (3) provides valuable insights. Interchain dipolar coupling results in the correlated creation of pairs of spin excitations of opposite momentum in each leg, with a momentum-dependent rate $\Omega_k = J\sum_j V_{0j}^{AB}e^{-ikj}$, whereas intrachain interaction leads to an effective band dispersion for the motion of spin excitations along the legs, $\varepsilon_k = J\sum_{j\neq 0} V_{0j}^{\alpha\alpha}e^{-ikj} = J(1 - 3\sin^2\theta)\sum_{j\neq 0} e^{-ikj}/|j|^3$. The Hamiltonian (3) can be diagonalized by means of a Bogoliubov transformation [57], yielding the eigenenergies $\xi_k = \sqrt{\varepsilon_k^2 - |\Omega_k|^2}$. Real ξ_k values lead to oscillatory dynamics $n_k^A(t) = n_{-k}^B(t) = (|\Omega_k|/\xi_k)^2\sin^2(\xi_k t)$. Crucially, ξ_k may become imaginary for certain momenta k_c, resulting in the dynamical instability of the spin pattern, triggering (at short times) the exponential growth of correlated spin excitations in both legs [43], $n_{k_c}^A(t) = n_{-k_c}^B(t) \propto (|\Omega_{k_c}|/|\xi_{k_c}|)^2 e^{2\Gamma_{k_c}t}$, with $\Gamma_{k_c} = \mathrm{Im}[\xi_{k_c}]$ being the growth rate of mode k_c. We define the instability rate as $\Gamma = \max_{k_c}\Gamma_{k_c}$. Figure 1(b) shows Γ as a function of Δ and θ for two different values of L.

The momentum-dependent interplay between intraleg dispersion and interleg pair creation is crucial for the stability of the initial spin pattern and, as shown below, also for the long-time evolution. Bogoliubov instability for a given quasimomentum k demands $|\epsilon_k| < |\Omega_k|$. Note that, whereas $|\Omega_k|$ decreases with the interchain separation Δ, the bandwidth associated with the intrachain dispersion ϵ_k is independent of Δ. As a result, except in the vicinity of the magic angle $\theta_M = \arcsin(1/\sqrt{3})$ discussed below, only $k \simeq k_0 \simeq 0.46\pi$, such that $\epsilon_{k_0} = 0$, contribute to the instability for large-enough Δ. However, for a finite chain with L sites, the quasimomentum takes only discrete values $\{k_j\}$. Therefore, for system sizes where k_0 cannot be reached, an effective threshold $\Delta_c(\theta, L)$ emerges [Fig. 1(b)], such that for $\Delta > \Delta_c$, $|\epsilon_{k_j}| > |\Omega_{k_j}|$ for all k_j, and hence the initial spin pattern is Bogoliubov stable. The situation is very different for $\theta \simeq \theta_M$, since $\epsilon_k = 0$ for all k, and hence ξ_k is imaginary for all quasimomenta. Instability is hence strongly enhanced, being maximal for $k = 0$, with $\Gamma \simeq \frac{4J}{3\Delta^2}$.

To put this into the context of false-vacuum decay, we see that the initial state is classically fully static, and the Bogoliubov analysis demonstrates it is quadratically stable

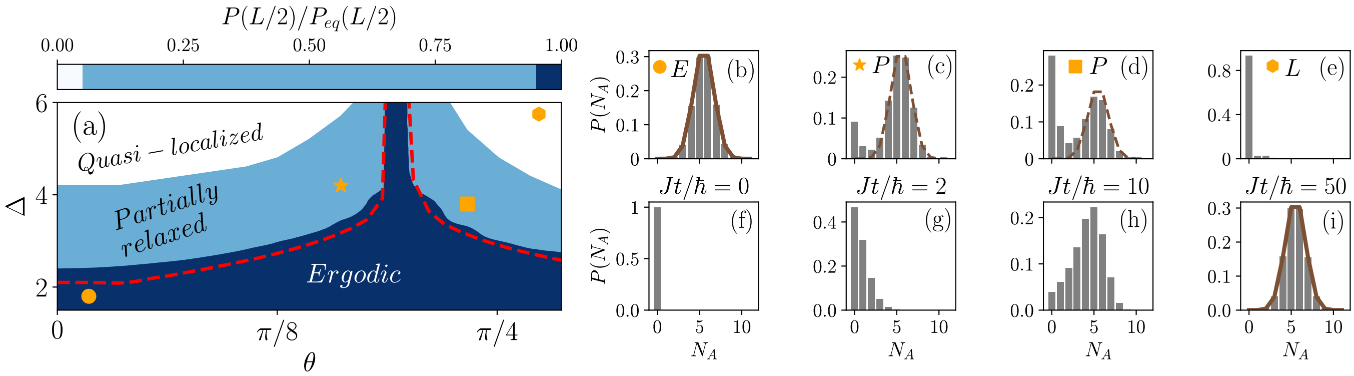

FIG. 2. (a) Ratio $P(L/2)/P_{\mathrm{eq}}(L/2)$ at a time $\bar{V}t = 50$ as a function of θ and Δ. In the ergodic (E) regime (dark blue), $1-\delta < P(L/2)/P_{\mathrm{eq}}(L/2) < 1$; in the the partially relaxed (P) regime (light blue), $\delta < P(L/2)/P_{\mathrm{eq}}(L/2) < 1-\delta$; and in the quasilocalized (L) regime (white), $0 < P(L/2)/P_{\mathrm{eq}}(L/2) < \delta$. We consider $\delta = 0.05$, but other reasonably small values of δ do not significantly alter the results. The dashed red curve corresponds to the Bogoliubov instability threshold. (b)–(e) Distribution of spin excitations $P(N_A)$ at four points in panel (a), indicated by markers. (f)–(i) Evolution towards thermalization of $P(N_A)$ for $\Delta = 2$ and $\theta = 0$. Brown solid curves indicate the equilibrium distribution (4). Dashed curves depict a rescaled Gaussian characterizing the partially relaxed regime. All plots are obtained using Chebyshev evolution for ladders with 11 rungs.

(for large layer separations), i.e., a local energy minimum within the mean-field analysis. Eventual relaxation therefore requires creation of spin excitations via quantum fluctuations. This is then directly analogous to quantum tunneling through a mean-field energy barrier leading to decay of a metastable false vacuum.

Magnetization imbalance and spin distribution. The stability analysis cannot describe the relaxation dynamics beyond the initial stages. We focus at this point on the long-time evolution, and in particular on whether the system behaves ergodically, reaching equilibrium. To this aim, we employ a Chebyshev expansion [57,59], which provides a numerically exact evolution for arbitrarily long times [60]. Due to its numerical complexity, we restrict to chains with $L = 11$ rungs. In order to characterize the relaxation dynamics, we monitor the imbalance $\eta = m_A - m_B$, where $m_{\sigma=A,B} = \frac{1}{L}\sum_{i=1}^{L}\langle\hat{s}^z_{i\sigma}\rangle$ is the magnetization of chain A (B). The imbalance is maximal, $\eta = 1$, for the initial condition and reaches $\eta = 0$ when the up and down spins are evenly admixed between the two chains. Note that $\eta = 1 - 2n_A$, with $n_A = N_A/L$ being the density of spin excitations in chain A ($N_A = \sum_i\langle\hat{a}_i^\dagger\hat{a}_i\rangle$).

A more detailed probe of the relaxation dynamics is provided by the full counting statistics $P(N_{\sigma=A,B})$ of the number of spin excitations within each chain. Due to energy conservation ($\langle\hat{H}\rangle = 0$ at any time), and the fact that spin-exchange preserves $m_A + m_B = 0$, we expect that, if ergodicity is reached, all states with a given number of excitations N_A along chain A and $N_B = N_A$ excitations along chain B are equally probable, irrespective of how the excitations are spatially distributed. The probability that chain A has N_A spin excitations, i.e., magnetization $m_A = 1/2 - N_A/L$, would hence be [57]

$$P_{\mathrm{eq}}(N_A) = \frac{\binom{L}{N_A}^2}{\binom{2L}{L}} \simeq \frac{2}{\sqrt{\pi L}}e^{-4(N_A-L/2)^2/L}. \tag{4}$$

Relaxation dynamics. In order to compare the spin dynamics for different Δ values, we gauge out the trivial stretching of the timescale of the dynamics associated with a growing Δ, by introducing the averaged interleg interaction $\bar{V} = |(1/L)\sum_{i,j}V_{ij}^{AB}| \simeq \frac{2J}{\Delta^2}\cos^2\theta$ and considering long times, $\bar{V}t \gg 1$ [61]. Figure 1(c) shows the evolution of the imbalance for $\theta = 0$ and different Δ values. For short times, numerical results are in very good agreement with the Bogoliubov prediction (red curves). At longer times, the hard-core nature of the spin excitations, neglected in the Bogoliubov analysis, becomes relevant. For $\Delta = 2$, for which the system is Bogoliubov unstable, homogenization is quickly reached. For $\Delta = 2.5$ and 6, the initial pattern is Bogoliubov stable, but beyond-Bogoliubov physics eventually results in relaxation, although with an exceedingly long-lived memory of the initial condition.

The long-time evolution reveals three distinct relaxation regimes, illustrated in Figs. 2(a)–2(e) for $\bar{V}t = 50$. In the ergodic regime, at low-enough Δ, the system relaxes into a fully balanced distribution ($\eta = 0$), and $P(N_A)$ reaches $P_{\mathrm{eq}}(N_A)$ [Fig. 2(b)]. Figure 2(a) shows $P(L/2)/P_{\mathrm{eq}}(L/2)$ as a function of θ and Δ; $P(L/2)/P_{\mathrm{eq}}(L/2) \simeq 1$ in the ergodic regime (dark blue region). As shown in Figs. 2(f)–2(i) for $\theta = 0$ and $\Delta = 2$, $P(N_A)$ rapidly approaches equilibrium, in a time of a few tens of $\hbar/J$, well within experimental reach. As expected from Bogoliubov analysis, short-time relaxation is characterized by the exponential creation of correlated pairs of spin excitations, and hence by an exponentially decreasing $P(N_A)$ [Fig. 2(g)], and the formation of a thermofield double state [62,63]. Eventually, further creation of excitations is arrested by their hard-core nature, and $P(N_A)$ transitions from an exponential to the Gaussian $P_{\mathrm{eq}}(N_A)$ already at $Jt/\hbar \simeq 50$ [Fig. 2(i)].

The long-time behavior presents similar qualitative features as the instability rate of Fig. 1(b). The enhanced Bogoliubov instability for $\theta \simeq \theta_M$ translates into ergodic dynamics even for large Δ. Moreover, as expected from the stability analysis, for large-enough Δ the system enters the quasilocalized regime, in which the spin distribution remains fully imbalanced, with $\eta \simeq 1$ and $P(N_A = 0) \simeq 1$ [Fig. 2(e)]. This regime is hence characterized by $P(L/2)/P_{\mathrm{eq}}(L/2) \simeq 0$ [white region in Fig. 2(a)]. We have checked that this remains so up to an eventual relaxation at exponentially long times, resembling

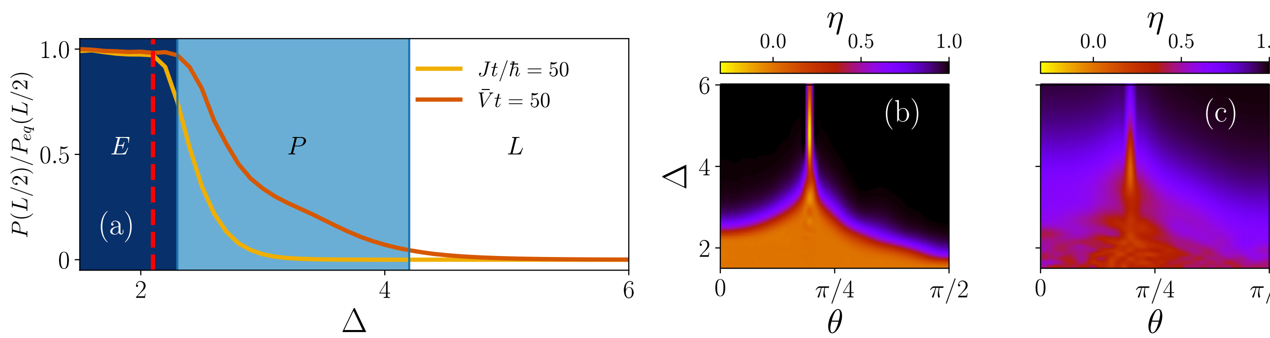

FIG. 3. (a) Ratio $P(L/2)/P_{\rm eq}(L/2)$ as a function of Δ for $\theta = 0$ at two different evolution times. The dashed red line corresponds to the Bogoliubov stability threshold. Colored regions indicate the ergodic (E), partially relaxed (P), and quasilocalized (L) regimes characterizing the long-time evolution. (b) and (c) Imbalance η after a time $Jt/\hbar = 50$ as a function of θ and Δ for a fully filled lattice and for sparse (25%) random filling, respectively. For all plots, we employ Chebyshev evolution for 11 rungs, except in panel (c), where we average over 100 realizations of 11 randomly placed spins in each leg of a 44-rung ladder.

the case of a metastable false vacuum [51]. However, over extremely long timescales $\propto 10^5 Jt/\hbar$, the spin distribution within the quasilocalized regime relaxes towards $P_{\rm eq}$.

Interestingly, at intermediate Δ values, the system enters a partially relaxed regime. $P(N_A)$ acquires a peculiar bimodal distribution [Figs. 2(c) and 2(d)]. Part of the distribution reaches a Gaussian dependence around $N_A = L/2$, as expected from ergodic evolution, whereas the rest remains peaked at $N_A = 0$, as in the quasilocalized regime. As a result, $0 < P(L/2)/P_{\rm eq}(L/2) < 1$ [light blue area in Fig. 2(a)]. The bimodal distribution is maintained for very long evolution times [57], well over any present or foreseeable experimental lifetimes, indicating the presence of eigenstates with very different degrees of ergodicity.

Experimental considerations. The abrupt ergodic to nonergodic crossover as a function of Δ characteristic of short evolution times may be readily probed using polar molecules or Rydberg atoms, as illustrated by our results at $Jt/\hbar = 50$ in Fig. 3(a), where we show $P(L/2)/P_{\rm eq}(L/2)$ as a function of Δ for $\theta = 0$ [see also Figs. 2(f)–2(i)]. Probing the partially relaxed regime demands longer evolutions such as $\bar{V}t = 50$ in Fig. 3(a). Note that for $\Delta = 3$, this corresponds to $Jt/\hbar \simeq 200$. Recent experiments on polar molecules have demonstrated rotational coherence times well over this timescale [64].

Experiments, especially those with polar molecules in optical lattices, are characterized by a sparse lattice filling [29,36], limited to less than 25%. Sparse filling results in random positions of the spins, which amounts to spatial disorder of the exchange couplings. Compared to the clean case depicted in Fig. 3(b), positional disorder, rather than localizing disorder, enhances instability and homogenization, as depicted in Fig. 3(c), where we show the imbalance at $Jt/\hbar = 50$ for a 25% filling. In contrast, our results show that typical disorder resulting from the differential polarizability and imperfections of the lattice or the tweezer array results in an almost negligible effect [57].

For the case we discussed, monitoring relaxation requires leg-resolved detection of one of the spin components. For polar molecules, this may be readily achieved by means of an electric field gradient perpendicular to the legs, which changes the energy splitting between the desired rotational states in each leg, allowing for leg-resolved spin-resolved measurements [41]. Recent advances in single-site resolution in polar molecules and magnetic and Rydberg atoms [23,36,65] further enable the possibility to study relaxation dynamics beyond the leg-polarized initial state considered here.

Conclusions. Dipolar spin ladders feature highly nontrivial relaxation dynamics due to the interplay between intra- and interleg interactions, which we have illustrated for the relevant case in which each leg is initialized in the opposite spin state. The dynamics have an intriguing dependence on the dipole orientation and the interchain separation, being maximally ergodic at the magic angle for which intrachain interactions vanish. Moreover, increasing the interleg spacing leads not only to the expected enlargement of time scales but also to a qualitative change in the stability of the initial pattern and in the long-term evolution, which falls into one of three possible regimes: ergodic, quasilocalized, and partially relaxed. We have checked that other initial states, accessible in the presence of single-site resolution, such as opposite spin orientations in even and odd rungs, result in qualitatively similar relaxation regimes. The predicted dynamics may be probed in current and near-future experiments.

Acknowledgments. We acknowledge useful feedback from H. Hirzler and S. Agarwal. L.S. and G.A.D.-C. acknowledge support of the Deutsche Forschungsgemeinschaft (DFG, German Research Foundation) under Germany's Excellence Strategy, EXC-2123 QuantumFrontiers, Grant No. 390837967. A.M.R. acknowledges support from the AFOSR MURI, ARO Grant No. W911NF-24-1-0128, NSF Grant No. JILA-PFC PHY-2317149, NSF Grant No. QLCI-2016244, the DOE Quantum Systems Accelerator (QSA), and the NIST.

[1] M. Schreiber, S. S. Hodgman, P. Bordia, H. P. Lüschen, M. H. Fischer, R. Vosk, E. Altman, U. Schneider, and I. Bloch, Observation of many-body localization of interacting fermions in a quasirandom optical lattice, Science **349**, 842 (2015).

[2] S. S. Kondov, W. R. McGehee, W. Xu, and B. DeMarco, Disorder-induced localization in a strongly correlated atomic Hubbard gas, Phys. Rev. Lett. **114**, 083002 (2015).

[3] J. Smith, A. Lee, P. Richerme, B. Neyenhuis, P. W. Hess, P. Hauke, M. Heyl, D. A. Huse, and C. Monroe, Many-body localization in a quantum simulator with programmable random disorder, Nat. Phys. **12**, 907 (2016).

[4] H. Bernien, S. Schwartz, A. Keesling, H. Levine, A. Omran, H. Pichler, S. Choi, A. S. Zibrov, M. Endres, M. Greiner *et al.*, Probing many-body dynamics on a 51-atom quantum simulator, Nature (London) **551**, 579 (2017).

[5] S. Scherg, T. Kohlert, P. Sala, F. Pollmann, B. Hebbe Madhusudhana, I. Bloch, and M. Aidelsburger, Observing non-ergodicity due to kinetic constraints in tilted Fermi-Hubbard chains, Nat. Commun. **12**, 4490 (2021).

[6] W. Morong, F. Liu, P. Becker, K. Collins, L. Feng, A. Kyprianidis, G. Pagano, T. You, A. Gorshkov, and C. Monroe, Observation of stark many-body localization without disorder, Nature (London) **599**, 393 (2021).

[7] S. Trotzky, P. Cheinet, S. Folling, M. Feld, U. Schnorrberger, A. M. Rey, A. Polkovnikov, E. A. Demler, M. D. Lukin, and I. Bloch, Time-resolved observation and control of superexchange interactions with ultracold atoms in optical lattices, Science **319**, 295 (2008).

[8] A. Mazurenko, C. S. Chiu, G. Ji, M. F. Parsons, M. Kanász-Nagy, R. Schmidt, F. Grusdt, E. Demler, D. Greif, and M. Greiner, A cold-atom Fermi–Hubbard antiferromagnet, Nature (London) **545**, 462 (2017).

[9] R. Brown, R. Wyllie, S. Koller, E. Goldschmidt, M. Foss-Feig, and J. Porto, Two-dimensional superexchange-mediated magnetization dynamics in an optical lattice, Science **348**, 540 (2015).

[10] D. Greif, G. Jotzu, M. Messer, R. Desbuquois, and T. Esslinger, Formation and dynamics of antiferromagnetic correlations in tunable optical lattices, Phys. Rev. Lett. **115**, 260401 (2015).

[11] R. A. Hart, P. M. Duarte, T.-L. Yang, X. Liu, T. Paiva, E. Khatami, R. T. Scalettar, N. Trivedi, D. A. Huse, and R. G. Hulet, Observation of antiferromagnetic correlations in the Hubbard model with ultracold atoms, Nature (London) **519**, 211 (2015).

[12] J. H. Drewes, L. A. Miller, E. Cocchi, C. F. Chan, N. Wurz, M. Gall, D. Pertot, F. Brennecke, and M. Köhl, Antiferromagnetic correlations in two-dimensional fermionic Mott-insulating and metallic phases, Phys. Rev. Lett. **118**, 170401 (2017).

[13] P. T. Brown, D. Mitra, E. Guardado-Sanchez, P. Schauß, S. S. Kondov, E. Khatami, T. Paiva, N. Trivedi, D. A. Huse, and W. S. Bakr, Spin-imbalance in a 2D Fermi-Hubbard system, Science **357**, 1385 (2017).

[14] I. Dimitrova, N. Jepsen, A. Buyskikh, A. Venegas-Gomez, J. Amato-Grill, A. Daley, and W. Ketterle, Enhanced superexchange in a tilted Mott insulator, Phys. Rev. Lett. **124**, 043204 (2020).

[15] M. A. Nichols, L. W. Cheuk, M. Okan, T. R. Hartke, E. Mendez, T. Senthil, E. Khatami, H. Zhang, and M. W. Zwierlein, Spin transport in a Mott insulator of ultracold fermions, Science **363**, 383 (2019).

[16] R. Lu, H. Sun, S. Kumar, Y. Wang, M. Gu, M. Zeng, Y.-J. Hao, J. Li, J. Shao, X.-M. Ma, Z. Hao, K. Zhang, W. Mansuer, J. Mei, Y. Zhao, C. Liu, K. Deng, W. Huang, B. Shen, K. Shimada *et al.*, Half-magnetic topological insulator with magnetization-induced Dirac gap at a selected surface, Phys. Rev. X **11**, 011039 (2021).

[17] S. Hirthe, T. Chalopin, D. Bourgund, P. Bojović, A. Bohrdt, E. Demler, F. Grusdt, I. Bloch, and T. A. Hilker, Magnetically mediated hole pairing in fermionic ladders of ultracold atoms, Nature (London) **613**, 463 (2023).

[18] A. de Paz, A. Sharma, A. Chotia, E. Maréchal, J. H. Huckans, P. Pedri, L. Santos, O. Gorceix, L. Vernac, and B. Laburthe-Tolra, Nonequilibrium quantum magnetism in a dipolar lattice gas, Phys. Rev. Lett. **111**, 185305 (2013).

[19] L. Chomaz, I. Ferrier-Barbut, F. Ferlaino, B. Laburthe-Tolra, B. L. Lev, and T. Pfau, Dipolar physics: a review of experiments with magnetic quantum gases, Rep. Prog. Phys. **86**, 026401 (2023).

[20] Y. A. Alaoui, B. Zhu, S. R. Muleady, W. Dubosclard, T. Roscilde, A. M. Rey, B. Laburthe-Tolra, and L. Vernac, Measuring correlations from the collective spin fluctuations of a large ensemble of lattice-trapped dipolar spin-3 atoms, Phys. Rev. Lett. **129**, 023401 (2022).

[21] L. Gabardos, B. Zhu, S. Lepoutre, A. M. Rey, B. Laburthe-Tolra, and L. Vernac, Relaxation of the collective magnetization of a dense 3D array of interacting dipolar $S = 3$ atoms, Phys. Rev. Lett. **125**, 143401 (2020).

[22] S. Lepoutre, J. Schachenmayer, L. Gabardos, B. Zhu, B. Naylor, E. Maréchal, O. Gorceix, A. M. Rey, L. Vernac, and B. Laburthe-Tolra, Out-of-equilibrium quantum magnetism and thermalization in a spin-3 many-body dipolar lattice system, Nat. Commun. **10**, 1714 (2019).

[23] L. Su, A. Douglas, M. Szurek, R. Groth, S. F. Ozturk, A. Krahn, A. H. Hébert, G. A. Phelps, S. Ebadi, S. Dickerson, F. Ferlaino, O. Marković, and M. Greiner, Dipolar quantum solids emerging in a Hubbard quantum simulator, Nature (London) **622**, 724 (2023).

[24] A. Patscheider, B. Zhu, L. Chomaz, D. Petter, S. Baier, A.-M. Rey, F. Ferlaino, and M. J. Mark, Controlling dipolar exchange interactions in a dense three-dimensional array of large-spin fermions, Phys. Rev. Res. **2**, 023050 (2020).

[25] A. Browaeys and T. Lahaye, Many-body physics with individually controlled Rydberg atoms, Nat. Phys. **16**, 132 (2020).

[26] P. Scholl, H. J. Williams, G. Bornet, F. Wallner, D. Barredo, L. Henriet, A. Signoles, C. Hainaut, T. Franz, S. Geier, A. Tebben, A. Salzinger, G. Zürn, T. Lahaye, M. Weidemüller, and A. Browaeys, Microwave engineering of programmable *xxz* Hamiltonians in arrays of Rydberg atoms, PRX Quantum **3**, 020303 (2022).

[27] Y. Chew, T. Tomita, T. P. Mahesh, S. Sugawa, S. de Léséleuc, and K. Ohmori, Ultrafast energy exchange between two single Rydberg atoms on a nanosecond timescale, Nat. Photon. **16**, 724 (2022).

[28] A. Signoles, T. Franz, R. Ferracini Alves, M. Gärttner, S. Whitlock, G. Zürn, and M. Weidemüller, Glassy dynamics in a disordered Heisenberg quantum spin system, Phys. Rev. X **11**, 011011 (2021).

[29] B. Yan, S. A. Moses, B. Gadway, J. P. Covey, K. R. Hazzard, A. M. Rey, D. S. Jin, and J. Ye, Observation of dipolar spin-exchange interactions with lattice-confined polar molecules, Nature (London) **501**, 521 (2013).

[30] J. L. Bohn, A. M. Rey, and J. Ye, Cold molecules: Progress in quantum engineering of chemistry and quantum matter, Science **357**, 1002 (2017).

[31] S. A. Moses, J. P. Covey, M. T. Miecnikowski, D. S. Jin, and J. Ye, New frontiers for quantum gases of polar molecules, Nat. Phys. **13**, 13 (2017).
[32] A. M. Kaufman and K.-K. Ni, Quantum science with optical tweezer arrays of ultracold atoms and molecules, Nat. Phys. **17**, 1324 (2021).
[33] Y. Bao, S. S. Yu, L. Anderegg, E. Chae, W. Ketterle, K.-K. Ni, and J. M. Doyle, Dipolar spin-exchange and entanglement between molecules in an optical tweezer array, Science **382**, 6675 (2023).
[34] C. M. Holland, Y. Lu, and L. W. Cheuk, On-demand entanglement of molecules in a reconfigurable optical tweezer array, Science **382**, 1143 (2023).
[35] J. T. Zhang, L. R. B. Picard, W. B. Cairncross, K. Wang, Y. Yu, F. Fang, and K.-K. Ni, An optical tweezer array of ground-state polar molecules, Quantum Sci. Technol. **7**, 035006 (2022).
[36] L. Christakis, J. S. Rosenberg, R. Raj, S. Chi, A. Morningstar, D. A. Huse, Z. Z. Yan, and W. S. Bakr, Probing site-resolved correlations in a spin system of ultracold molecules, Nature (London) **614**, 64 (2023).
[37] M. Atala, M. Aidelsburger, M. Lohse, J. T. Barreiro, B. Paredes, and I. Bloch, Observation of chiral currents with ultracold atoms in bosonic ladders, Nat. Phys. **10**, 588 (2014).
[38] Y. Ye, Z.-Y. Ge, Y. Wu, S. Wang, M. Gong, Y.-R. Zhang, Q. Zhu, R. Yang, S. Li, F. Liang, J. Lin, Y. Xu, C. Guo, L. Sun, C. Cheng, N. Ma, Z. Y. Meng, H. Deng, H. Rong, C.-Y. Lu *et al.*, Propagation and localization of collective excitations on a 24-qubit superconducting processor, Phys. Rev. Lett. **123**, 050502 (2019).
[39] M. Gall, N. Wurz, J. Samland, C. F. Chan, and M. Köhl, Competing magnetic orders in a bilayer Hubbard model with ultracold atoms, Nature (London) **589**, 40 (2021).
[40] J. F. Wienand, S. Karch, A. Impertro, C. Schweizer, E. McCulloch, R. Vasseur, S. Gopalakrishnan, M. Aidelsburger, and I. Bloch, Emergence of fluctuating hydrodynamics in chaotic quantum systems, Nat. Phys. (2024), doi:10.1038/s41567-024-02611-z.
[41] W. G. Tobias, K. Matsuda, J.-R. Li, C. Miller, A. N. Carroll, T. Bilitewski, A. M. Rey, and J. Ye, Reactions between layer-resolved molecules mediated by dipolar spin exchange, Science **375**, 1299 (2022).
[42] T. Bilitewski and A. M. Rey, Manipulating growth and propagation of correlations in dipolar multilayers: From pair production to bosonic Kitaev models, Phys. Rev. Lett. **131**, 053001 (2023).
[43] T. Bilitewski, G. A. Domínguez-Castro, D. Wellnitz, A. M. Rey, and L. Santos, Tunable momentum pair creation of spin excitations in dipolar bilayers, Phys. Rev. A **108**, 013313 (2023).
[44] G. Agarwal, *Quantum Optics* (Cambridge University, Cambridge, England, 2013).
[45] Z. Tian, S.-Y. Chä, and U. R. Fischer, Roton entanglement in quenched dipolar Bose-Einstein condensates, Phys. Rev. A **97**, 063611 (2018).
[46] M. Rigol, V. Dunjko, V. Yurovsky, and M. Olshanii, Relaxation in a completely integrable many-body quantum system: An *ab initio* study of the dynamics of the highly excited states of 1D lattice hard-core bosons, Phys. Rev. Lett. **98**, 050405 (2007).
[47] D. A. Abanin, E. Altman, I. Bloch, and M. Serbyn, *Colloquium:* Many-body localization, thermalization, and entanglement, Rev. Mod. Phys. **91**, 021001 (2019).
[48] A. P. Luca D'Alessio, Y. Kafri, and M. Rigol, From quantum chaos and eigenstate thermalization to statistical mechanics and thermodynamics, Adv. Phys. **65**, 239 (2016).
[49] K. Mallayya, M. Rigol, and W. De Roeck, Prethermalization and thermalization in isolated quantum systems, Phys. Rev. X **9**, 021027 (2019).
[50] A. Bastianello, A. D. Luca, and R. Vasseur, Hydrodynamics of weak integrability breaking, J. Stat. Mech.: Theory Exp. (2021) 114003.
[51] S. Coleman, Fate of the false vacuum: Semiclassical theory, Phys. Rev. D **15**, 2929 (1977).
[52] G. Lagnese, F. M. Surace, M. Kormos, and P. Calabrese, False vacuum decay in quantum spin chains, Phys. Rev. B **104**, L201106 (2021).
[53] A. Milsted, J. Liu, J. Preskill, and G. Vidal, Collisions of false-vacuum bubble walls in a quantum spin chain, PRX Quantum **3**, 020316 (2022).
[54] A. Zenesini, A. Berti, R. Cominotti, C. Rogora, I. G. Moss, T. P. Billam, I. Carusotto, G. Lamporesi, A. Recati, and G. Ferrari, False vacuum decay via bubble formation in ferromagnetic superfluids, Nat. Phys. **20**, 558 (2024).
[55] R. Steinigeweg, F. Heidrich-Meisner, J. Gemmer, K. Michielsen, and H. De Raedt, Scaling of diffusion constants in the spin-$\frac{1}{2}$ XX ladder, Phys. Rev. B **90**, 094417 (2014).
[56] T. Rakovszky, C. W. von Keyserlingk, and F. Pollmann, Dissipation-assisted operator evolution method for capturing hydrodynamic transport, Phys. Rev. B **105**, 075131 (2022).
[57] See Supplemental Material http://link.aps.org/supplemental/10.1103/PhysRevA.110.L021302 for a detailed discussion of the Bogoliubov analysis, the Chebyshev method, the equilibrium distribution, the entanglement entropy, and extended numerical results.
[58] Note that quantum fluctuations are crucial to trigger the spin dynamics. In classical spins, the vacuum state would not evolve.
[59] H. Fehske, R. Schneider, and A. Weisse, *Computational Many-Particle Physics*, Lecture Notes in Physics (Springer, Berlin, 2007), Vol. 739.
[60] Although a semiclassical method such as the discrete truncated Wigner approach satisfactorily reproduces the short-term dynamics, it tends to underestimate the relaxation time, pointing to the building up of higher-order correlations.
[61] In order to avoid very long timescales resulting from the vanishing angular dependence of $\bar{V}$, we restrict the long-time analysis to orientations with $0 < \theta < 0.9\pi$.
[62] Y. Takahashi and H. Umezawa, Thermo field dynamics, Int. J. Mod. Phys. B **10**, 1755 (1996).
[63] S. Chapman, J. Eisert, L. Hackl, M. P. Heller, R. Jefferson, H. Marrochio, and R. C. Myers, Complexity and entanglement for thermofield double states, SciPost Phys. **6**, 034 (2019).
[64] P. D. Gregory, L. M. Fernley, A. L. Tao, S. L. Bromley, J. Stepp, Z. Zhang, S. Kotochigova, K. R. A. Hazzard, and S. L. Cornish, Second-scale rotational coherence and dipolar interactions in a gas of ultracold polar molecules, arXiv:2306.02991.
[65] G. Bornet, G. Emperauger, C. Chen, F. Machado, S. Chern, L. Leclerc, B. Gély, D. Barredo, T. Lahaye, N. Y. Yao, and A. Browaeys, Enhancing a many-body dipolar Rydberg tweezer array with arbitrary local controls, Phys. Rev. Lett. **132**, 263601 (2024).